Role of the slow diffusion species in the dewetting of compounds: The case of NiSi on a Si isotope multilayer studied by atom probe tomography

T. Luo, Christophe Girardeaux, H. Bracht, Dominique Mangelinck

Role of the slow diffusion species in the dewetting of compounds: the case of NiSi on a Si isotope multilayer studied by atom probe tomography

T. Luo[1], C. Girardeaux[1], H. Bracht[2] and D. Mangelinck[3, a)]

[1] *Aix-Marseille University, CNRS, IM2NP, Faculté Saint Jérôme, Case 142, 13397 Marseille Cedex 20, France*

[2]*Institute of Materials Physics, Westfälische Wilhelms-Universität Münster, 48149 Münster, Germany*

[3]*CNRS, Aix-Marseille University, IM2NP, Faculté Saint Jérôme, Case 142, 13397 Marseille Cedex 20, France*

Abstract: Dewetting or agglomeration is a crucial process in material science since it controls the stability of thin films or can be used for film nanostructuration by formation of islands. The models developed for dewetting usually assume diffusion at the interface and/or at the surface but no direct evidence of such diffusion was demonstrated. Moreover, these models are usually dealing with elemental materials and not with compounds in which several elements can diffuse. The mechanisms behind agglomeration of polycrystalline compounds thin film are still not fully understood. In this work, Si isotope multilayers coupled with atom probe tomography (APT) are used to reveal the agglomeration mechanism of NiSi, a binary compound. The diffusion of Si, the less mobile species in NiSi, at the NiSi/Si interface is demonstrated through comparison between the three dimension redistribution of the Si isotopes determined by APT and models taking into account grooving and agglomeration. The implication for the understanding and control of agglomeration in poly-crystalline compound thin films are highlighted.

[a)] Corresponding author, e-mail: dominique.mangelinck@im2np.fr

Keywords: dewetting, NiSi compound, atom probe tomography, Si isotope, interface diffusion

1. Introduction

Thin solid films with submicron thicknesses may break up into islands to lower the free energy during high-temperature treatments. This phenomenon, termed “agglomeration” or ‘‘dewetting’’, is driven by the minimization of the total energy, including the film surface energy, the substrate surface energy and the film-substrate interfacial energy. For thin films, the large ratio of surface/volume induces a high driving force for agglomeration and films with low thicknesses are more prone to agglomerate. This is of particular concern in microelectronics for contacts, [1][2] and silicon-on-insulator (SOI) structures. [3] [4] Alternatively, solid state dewetting can be purposely used to obtain nanostructures and is of great interest in several applications including the self-assembly of nano-materials and/or nano-structuration. [5] [6] [7] [8]

A large amount of works has thus been driven by the technological importance of the dewetting phenomenon and an increasing research effort has been made during the last few years. [9] [10] The first theoretical approach developed by Mullins [11] is based on a continuum model for surface diffusion at the grain boundary-surface groove and predicts the formation of a smooth dewetting rim at the edge of the film. More global approaches have also been developed to predict the conditions and/ or the kinetics of agglomeration for polycrystalline films. [12] [13] [14] [15]

The discovery and study of dewetting of single-crystal films [9] [10] have driven the development of advanced models, giving new insights into the dewetting process. Although the dewetting process is quite complex and depends on many factors, it involves some of the

following steps [9] [10]: i) nucleation and growth of the holes on defects (edges of the films, grain boundaries for polycrystalline film, preexisting holes…), ii) hole expansion, usually with a propagating rim that may be rounded or facetted, iii) transformation of the rim into isolated islands due to Rayleigh instabilities.

This sequence of steps is especially true for mono-crystalline films but the diversity of studied systems leads to a wide panel of behaviors and mechanisms. [9] [10] Dewetting can exhibit numerous morphologies that strongly depend on the system (crystalline / amorphous substrates, films in epitaxy on single-crystals, polycrystalline films…). For films grown on single crystals, complex geometrical patterns and fractal features constrained by surface energy anisotropy can be observed while less regular shapes are found for polycrystalline films. In this regard, it is difficult to set up a unique model that applies to any system. In particular for polycrystalline films, grain growth also appears to play an important role and dewetting is related to the grain assembly evolution. [16] [17] [18] [19] It was also found that this evolution is related to diffusion at interfaces and grain boundaries that might be affected by the atmosphere used during the heat treatment. [19] [20] [21] Moreover, most models have been developed for mono-component films and fewer models are known about dewetting of compounds such as silicide where two (or more) elements can play different roles.

Dewetting of metal silicides is of particular concern for contacts in microelectronics and much research has been carried out to characterize and suppress dewetting.[2] [15] [22] [23] [24] [25] [26] NiSi is largely used as contacts for advanced devices and agglomeration of NiSi films is the main degradation mechanism when the Ni thickness <15nm.[2] Many factors could affect the agglomeration of NiSi films, such as the thickness of Ni, the type of the Si substrate, the grain size and the texture of NiSi. Deduytche et al. [2] used in-situ sheet resistance and in-situ laser light-scattering measurements to derive the activation energy for NiSi agglomeration on mono-crystalline Si and poly-crystalline Si. They found that the

agglomeration of NiSi is faster on mono-crystalline silicon than on poly-crystalline Si and this was attributed to a special texture called axiotaxy.[27] Axiotaxy occurs when a plane in the film is preferentially aligned to a plane with the same *d* spacing in the substrate, resulting in an interface that is periodic along one direction and that can thus more easily bend during agglomeration.[2] The addition of alloying element in NiSi was found to be efficient to limit agglomeration.[28] [29] [30] [25] Two main mechanisms were proposed for the effect of alloying element on agglomeration: change in texture [31] and/or change in diffusion along interface and grain boundaries.[26][32] However, experimental studies, to our knowledge, have not yet demonstrated direct evidence for diffusion at interface during agglomeration, and most studies have been focused on some factors influencing agglomeration, lacking the investigation on the fundamental mechanism of the NiSi agglomeration. Furthermore, NiSi is a binary compound in which one of the elements (Si) diffuses much more slowly than the other element (Ni). The exact agglomeration mechanism is still not known while the study of it could offer particular insights to the agglomeration mechanism of such poly-crystalline compounds.

In this work, silicon isotope multilayers and atom probe tomography (APT) are used to investigate the mechanism of agglomeration for the Ni monosilicide. Atom probe tomography is a powerful technique. The redistribution of the Si isotopes, both in NiSi and in the Si substrate, is determined by APT which can map out the distribution of atoms in three dimensions (3D) and distinguish between different isotopes with an atomic resolution. Direct experimental evidence for Si diffusion along the NiSi/Si interface is provided, giving an access to the agglomeration mechanism of NiSi thin films. Models that establish diffusion paths during the agglomeration process are developed. The role of the slow-diffusion element in compounds, such as silicide, is highlighted.

2. Experimental

Twenty undoped alternating ($^{30}Si/^{28}Si$)-bilayers were grown by means of molecular beam epitaxy (MBE) at 650°C on top of a (100)-oriented p-type CZ-Si wafer with a specific resistivity of 6.5 Ohm cm.

The thickness of each bilayer, one layer enriched with ^{30}Si and one layer enriched with ^{28}Si, is about 17nm. Two kinds of substrates, natural and isotope Si, were immersed into 5% HF for 1 min to remove the native oxide prior to the deposition. Afterwards, 15nm Ni was deposited on natural and isotope Si(001) simultaneously by magnetron sputtering at room temperature. The pressure is lowered to ~10^{-8} Torr prior to the injection of 99.99% pure Ar. The deposition rate as a function of power is calibrated for the Ni target. The applied power on the Ni target is 150W and the corresponding deposition rate is 0.3555 nm/s.

In-situ XRD measurement was performed on the as-deposited Ni/Si(natural) sample from 150°C to 400°C in the Bragg-Brentano geometry. The pressure of the XRD vacuum chamber is ~10^{-6} Torr. Temperature was firstly increased from room temperature to 150°C at a speed of ~35°C/min. From 150°C to 400°C, temperature was increased by steps of 5°C at a speed of 10°C/min, and a 4min-XRD scan was performed after each step.

Rapid thermal processing (RTP) was used to anneal samples at 600°C for 60s under vacuum (~10^{-6} Torr). The annealed sample was observed by a scanning electron microscopy (SEM, Zeiss GeminiSEM 500 ultra-high resolution FESEM), which is equipped with a backscattered electron (BSE) detector as well as an energy dispersive X-ray spectroscopy (EDS) system. The sample surface topography was studied using an NT-MDT SMENA atomic force microscope (AFM) in air under ambient conditions in a non-contact mode.

Needle-shaped specimens were prepared on the annealed sample in the direction perpendicular to the sample surface by focused ion beam (FIB) equipped with a micromanipulator. The detailed sample preparation procedure has been described elsewhere. [33] Note that a Ni protection layer of ~100nm is usually deposited on the sample surface prior to the FIB processing to avoid contamination of Ga^+ ions. Ni was chosen because it has a better adhesion and better field evaporation characteristics in APT for these Ni silicide samples. This step is especially crucial for thin films: the Ni protection layer usually contains a high content of oxygen and could be easily distinguished, in our case, from the original 15nm Ni film. The final APT tip is usually prepared in order to leave a small part of the Ni protection layer on top: this ensures that the initial sample surface (before the deposition of the Ni protection layer) is included in the APT volume. The APT analyses were carried out in a LEAP 3000X HR instrument. The laser pulsing rate was 100 kHz and the detection rate was kept at 0.002 event/pulse. The pressure in the analysis chamber is ~10^{-11} Torr. The specimen temperature was 50K and the laser energy was set as 0.8 to 1.3nJ. Data reconstructions were performed with the commercial IVAS software.

3. Results

The APT volume of an as-deposited 15nm/Si sample and the corresponding depth profile are shown in Figure 1. Three regions are observed: the Ni protection layer on the top, the as-deposited 15nm Ni film in the middle and the Si isotope multilayer at the bottom. As described in the “Experimental” section, prior to the FIB processing, the final APT tip usually contains a thin part of the Ni protection layer. High contents of NiO and O are found in this Ni protection layer (Figure 1b-①), making it easy to be distinguished from the as-deposited 15nm pure Ni (Figure 1b-②). However, as the Ni protection layer is not part of the real

sample, it is only displayed in the APT volume of the as-deposited sample (Figure 1) and will not be shown in the APT volumes of the 600°C-annealed sample (Figure 4-6). The expected thickness of the consumed Si isotope multilayer by the 15nm Ni film for the NiSi formation is marked in Figure 1b-③. Indeed due to the volume change during the reaction Ni+Si→NiSi [34], a 15nm Ni layer is expected to consume ~27 nm Si to form ~33 nm NiSi before the occurrence of NiSi agglomeration. Since a ^{30}Si rich layer was present at the initial Si surface, about two ^{30}Si rich layers and one ^{28}Si rich layer should be consumed by the formation of NiSi.

The in-situ XRD measurement of a 15nm Ni/Si from 150°C to 400°C is shown in Figure 2a. Metal-rich phases form firstly and the as-deposited Ni film is fully consumed at ~210°C. From 305°C, NiSi is the unique silicide on top of the Si substrate. The top-view BSE image and the corresponding EDS map of Ni element of the 600°C-annealed sample are shown in Figure 2b and c. The morphology of the agglomerated sample is characterized by the presence of two regions (Figure 2b): the dark region corresponds to the exposed Si substrate and the grey region to the agglomerated NiSi as evidence by the EDS map of Ni shown in Figure 2c. Some brighter green regions can also be observed in the EDS map of Ni (Figure 2c), which results from a larger Ni signal intensity. This increase in the Ni signal intensity should be due to a thicker NiSi film in these regions since EDS usually scans a thickness of more than 1μm. Therefore, the extent of agglomeration (or the thickness of NiSi) could be different for different grains. In Figure 2d, a schematic showing the formation, the grain boundary grooving and the agglomeration of the NiSi film is presented.

The AFM measurement was performed on the 600°C-annealed sample and the average roughness (root mean square) of the sample surface is ~2nm, which is much smaller than the thickness of the non-agglomerated NiSi film (~33nm). It indicates that the height of the

exposed Si region is similar to that of the NiSi region. This is in accordance with the cross-sectional TEM image of a 20nm Ni/Si sample after annealing at 750 °C for 30s [35]. Indeed, it has been reported [2,35,36] that the sample surface after the agglomeration of NiSi is relatively flat while the NiSi/Si interface is largely curved, and there are no holes in the agglomerated NiSi films. This can be understood by taking into account the volume change associated with the formation of NiSi as illustrated in Figure 3. This schematic aims to explain why there are no holes but only exposed Si region in the agglomerated NiSi film.

Even though dewetting or agglomeration usually induces curved interface (or surface), only a rectangular grain is considered to explain the absence/formation of holes (Figure 3). For simplicity, we thus assume that the NiSi grain maintains a rectangular shape before and after agglomeration. In Figure 3a, the A1 or A3 region refers to one quarter area (or volume) of the NiSi grain. If the agglomeration of a NiSi film results in the exposure of Si with 50% area, Ni atoms in A1 and A3 would diffuse away and form NiSi underneath A2. In the reaction of Ni+Si→NiSi, the volume ratio between the consumed Si to the formed NiSi is 0.85:1, which is calculated based on the conservative of matter and the atomic volume [34]. The height of the agglomerated NiSi surface is only slightly higher than the exposed Si. Considering the spherical shape of the agglomerated NiSi and the fact that less than 50% area of Si is exposed, the difference in the height is even smaller and only a small roughness is associated with the surface. Therefore, there are rather exposed Si regions than real holes in the agglomerated NiSi sample.

For comparison, the classical dewetting process of a mono-component material (X) on an undeformed substrate is also presented in Figure 3b. The position of the original film/substrate interface does not move due to the absence of reaction. The agglomerated film (X) is two times the height of the original film thickness (h) and the film surface is much higher than the exposed substrate, resulting in the formation of holes.

Figures 4 to 6 present five APT volumes that are typical of different regions of the 15nm Ni/isotope multilayer Si(001) annealed at 600°C. Several tips were analyzed from each of these regions but only the more representative ones are presented.

Figure 4 shows two APT volume where only the Si phase is present. The APT volume in Figure 4a originates from a tip prepared by FIB deep in the sample. A stack of isotope multilayers can be clearly seen in the volume (Figure 4a) and in the associated depth profile (Figure 4b). The period of the multilayer is ~17 nm and the interface are sharp except for the broadening linked to the APT measurement (about 2 nm [37]). Indeed a broadening is usually associated with the experimental depth profile of an interface even if this interface is atomically sharp and perfectly flat. This interface broadening may have several causes, including classical phenomena such as interface roughness and information depth, but also atom probe linked phenomena such as surface diffusion, preferential evaporation, differences in the evaporation field, or other causes linked to the data analysis (positioning of the sub-volume, binning, etc.) [38]. The interface broadening linked to APT can be estimated to be of a few nanometers [37] [38]. In order to accurately determine the composition and the thickness of the layers, the nominal composition profile convoluted with a Gaussian having a full width at half maximum of 2nm was compared to the APT profile of Figure 4b. The fitted thickness of the layers rich in ^{28}Si and ^{30}Si are 5.5 nm and 11.5 nm and their fitted composition expressed as (%^{28}Si : %^{29}Si : %^{30}Si) are (89 : 2 : 9) and (4 : 9 : 87) respectively. In this procedure, sharp interfaces were taken for the multilayer meaning that no self-diffusion of Si occurs at this low temperature [39]. Furthermore, the isotope depth profiles obtained in APT are similar for the as-deposited sample (Figure 1b) and the 600°C-annealed sample (Figure 4 b).

Figure 4c and d correspond to a zone of the sample where the Si surface is exposed. While the isotope multilayer structure is preserved deep in the sample, the concentration of the Si

isotopes is constant on a depth of about 30 nm. This concentration corresponds to the average composition of a bi-layer (31%^{28}Si:7%^{29}Si: 62%^{28}Si) and a full mixing of the Si isotopes has thus occurred in this region. In the following, the terms “mixed region” and “layered region” will be used to refer to the region, either in NiSi or in the Si substrate, where the Si isotopes are mixed or maintain the multilayer structure, respectively. The mixed Si layer is thus about 30 nm thick, which is slightly higher than the expected thickness of Si (~27nm) consumed by the 15 nm Ni film for the NiSi formation.

It appears thus that this Si region with a full mixing of the Si isotopes in Figure 4c and d derived from the former NiSi layer through the process of agglomeration. As the self-diffusion of Si inside the Si substrate is negligible at 600°C, the mixing of Si isotopes may occur by self-diffusion of Si either in the bulk of NiSi or at the NiSi/Si interface.

However, in the APT volume shown in Figure 5a and b, a layer of NiSi is present on the top and the multilayer structure is maintained in NiSi over ~30nm from the sample surface. This is an indication that full mixing does not occur in the bulk of NiSi before the occurrence of agglomeration even if the broadening of isotope profiles in this region reveals some self-diffusion of Si in NiSi. In order to quantify this diffusion, finite difference simulation of the diffusion was performed in one dimension using null fluxes as the boundary condition and the profile shown in Figure 4b as the initial profile. The simulated profile for ^{30}Si is superimposed on the experimental one in Figure 5b. From this simulation, the self-diffusion coefficient of Si in NiSi was fitted to be 0.09±0.02nm^2/s at 600°C. The APT analysis in Figure 5a and b also shows two other interesting features concerning the isotope redistribution: i) the multilayer structure is maintained in Si in contact with NiSi, and ii) there is a total mixing region of Si isotopes over a thickness of about 10nm in NiSi close to Si. In Figure 5a and b, as the NiSi/Si interface is not parallel to the multilayer interfaces but tilted with an angle, the film thickness varies with the region of interest. However, on average, the depth of the NiSi/Si interface is

larger than the original thickness of the non-agglomerated NiSi film. This local increase in thickness should be related to agglomeration.

A tilted NiSi/Si interface is also observed in Figure 5c and d, but the NiSi thickness ranges between 25 and 29 nm and is smaller than the one expected for non-agglomerated NiSi (i.e. 33nm). NiSi appears to be fully layered and there is a mixed Si layer of about 10 nm in contact with NiSi.

The APT volume shown in Figure 6 reveals a more complex structure in which a NiSi grain meets the Si substrate at the sample surface. The NiSi/Si interface is bent with a relatively large curvature close to the sample surface. The curvature is much smaller close to the NiSi surface / Si surface junction. This means that the area of the NiSi/Si interface is much larger than the area of the NiSi surface and it indicates that the NiSi surface energy is larger than the NiSi/Si interface energy. If this situation at the triple junction (NiSi-Si-vacuum) corresponds to an equilibrium state, the energy of the NiSi/Si interface is thus smaller than the surface energies for both NiSi and Si as indicated by the schematic in Figure 6a. Concerning the isotopes, NiSi presents a layered structure (Figure 6b) and is in contact with mixed Si all over the interface (Figure 6c). Below the Si mixed layer, the isotope multilayer is unchanged.

The results obtained from the APT volumes in Figure 4 to 6 are summarized in the schematic shown in Figure 7. An agglomerated NiSi grain, the distribution of Si isotopes and the locations corresponding to the different APT volumes are displayed. As the preparation of each APT tip requires a region of $2.5 \times 2.5\ \mu m^2$, it is not possible to fabricate several tips in a same grain since the grain size is about 200-500nm. On the other hand, the volume of a grain is too large to be included in one tip. The extent of agglomeration (or the maximum thickness of NiSi) could be different for different grains, but the APT results obtained on several grains are representative of the dewetting behavior. Figure 7 aims to schematically summarize all the APT results on a single grain even if the APT volumes were obtained from different grains.

Figure 7 only considers the status of Si isotopes, whether they are mixed or they maintain a layer structure in NiSi and Si. On the basis of these results, it appears that the redistribution of Si isotopes is linked to agglomeration.

4. Discussion

In order to better understand the experimental results, a model for the grooving and agglomeration of a compound is now developed under the following conditions: i) the diffusion of Ni is fast in NiSi, ii) the lattice diffusion of Si in NiSi and in Si is limited, and iii) the diffusion of Si is fast at the NiSi/Si interface. Ni atoms are thus expected to diffuse away from the top NiSi layer and to react with the Si atoms beneath the film, leading to the exposure of some Si regions and a larger thickness of NiSi. The model is based on the observation that the mixing of the isotopes occurs along the NiSi/Si interfaces. The mixed regions are assumed to correspond to the former position of the NiSi/Si interface and the layered structure is maintained in the region that were not swept by the interface. The volume of the NiSi grain was also assumed to be constant during agglomeration (i.e. no grain growth). The atomic volume of Si is taken as the double of the one of NiSi as the exact atomic volumes are 20 nm^3 and 12 nm^3 respectively. Under these last two assumptions, the law of conservation of mass is equivalent to the conservation of volume (i.e. the volume of Si released by agglomeration is equal to the volume of agglomerated NiSi).

Several geometries, in two dimensions (facetted grain, circular segment), were considered for the agglomerated grains. For the 2D geometries, the length in the depth dimension is considered to be constant (i.e. in the plane normal to the NiSi/Si interface) to simplify the analysis and to be closer to the APT observations. In these cases, the conservation of volumes can be transformed to the conservation of area.

As an example, the circular segment geometry will be detailed in a first place. As described in the schematics of Figure 8 a and b, the area A_1 (area of Si that was NiSi before agglomeration and becomes again Si after agglomeration) is taken equal to the surface A_2 (area of the newly created NiSi) and can be expressed as a function of A_2 and A_3 (area of the circular segment)

$$A_1 = L_g h_1 - (A_3 - A_2) = A_2 \Leftrightarrow L_g h_1 - A_3 = 0 \qquad \text{Eq. 1}$$

where L_g is the half size of the NiSi grain, and h_1 is the depth of the grain boundary grooving (Figure 8a).

Since A_3 can be expressed as a function of θ and L_g:

$$2A_3 = R^2\left(\theta - \cos\theta \sin\theta\right) \Leftrightarrow \left(\frac{L_g}{\sin\theta}\right)^2 \left(\theta - \cos\theta \sin\theta\right) = L_g{}^2\left(\theta / \sin\theta^2 - \cos\theta / \sin\theta\right)$$

where R is the radius of the NiSi/Si interface curvature, and θ is the angle defining the circular segment geometry (Figure 8).

One obtains the following relationship for the grooving:

$$2h_1 \sin^2\theta - L_g\left(\theta - \cos\theta \sin\theta\right) = 0 \qquad \text{Eq. 2}$$

A similar equation can be obtained for agglomeration using the same assumptions and the geometry shown in Figure 8b:

$$2h_g L_g \sin^2\theta - \left(L_g - L_{ag}\right)^2\left(\theta - \cos\theta \sin\theta\right) = 0 \qquad \text{Eq. 3}$$

where h_g is the original thickness of the non-agglomerated NiSi film and L_{ag} corresponds to the agglomerated length as indicated in Figure 8b.

To simulate the mixing of Si isotopes during grooving, the grooving height (h_1) was increased by small steps ($dh_1 << h_g$) and Eq. 2 was solved numerically to determine the position of the NiSi/Si interface. For the agglomeration, the length of agglomeration (L_{ag}) was increased by

small steps ($dL_{ag} << L_g$) and Eq. 3 was solved. The track of this interface was recorded at each step and has been drawn in Figure 8c, d and e.

One can see that this simple model allows to reproduce our main experimental results from APT. The models with the other geometries give similar results (the 2D model for a faceted NiSi grain is shown in Figure 8f and g) but match the experimental results to a lesser extent.

These simple models allow us to reproduce the main results concerning the redistribution of the Si isotopes. As pointed out before, the main assumption is that self-diffusion of Si occurs mainly at the NiSi/Si interface. The good match between simulation and experiments shows that diffusion along the interface of the slow diffusion species is crucial for agglomeration. Most of the models developed for dewetting are based on diffusion at surface or interface [11] [12] [13] [40] [41]. Especially it was pointed out that interface diffusion is playing a role for dewetting of polycrystalline thin film [16] [42] and that a change in annealing atmosphere can modify the mechanisms of dewetting by changing the contribution of interface diffusion [21] [19]. However, no direct experimental evidence for this interface diffusion has been demonstrated before our work. Moreover, most of these models deal with mono-component system [9] [10]. Our work, considering a binary compound, demonstrates that the diffusion of the slow diffusing species is concomitant to grooving and agglomeration. In the case of the monosilicide, the diffusion of Ni is effective in NiSi at temperatures as low as 250-300°C when the growth of NiSi occurs and it cannot be the limiting step at even higher temperatures (500-600°C for 15 nm NiSi film) when grooving and agglomeration occur. The limiting phenomena for grooving and agglomeration are thus the diffusion of the slow species (Si for NiSi) even if Si might be fully available from the substrate. The stronger Si-Si bond in the Si diamond structure than the one in the NiSi/Si interface could be the reason for this behavior. A rough estimation of the Si diffusion at the NiSi/Si interface as the square of the average half size of agglomerated grain (250 nm) over the time of the heat treatment gives a value of 1000

nm^2/s at 600°C. At 600°C, Si diffusion along the NiSi/Si interface is thus about 4 orders of magnitude faster than the bulk Si diffusion in NiSi and 14 orders of magnitude faster than the self-diffusion of Si (2×10^{-11} nm^2/s) [39]. The fact that agglomeration is developed along the NiSi/Si interface and not at the surface can be a consequence of the volume change or of higher surface energies than the interfacial energy as pointed before, but it might be also related to a faster diffusion of Si in the NiSi/Si interface than at the surface of NiSi or more precisely at the NiSi/oxide interface since the surface of NiSi is usually oxidized.

Dewetting is certainly a more complex process than the simple model developed here. Even for model systems such as epitaxial film on mono-crystalline substrate, complex phenomena such as Rayleigh instabilities, fractal behavior… have been observed. For poly-crystalline film, a much complex behavior is acting and grain growth, as well as the evolution of grain assembly are of importance. Moreover, the texture of the film is also expected to play an important role. In a polycrystalline film, grains can be randomly oriented or they can exhibit some special relationships with the substrate, such as epitaxy and axiotaxy. All these texture components may behave differently with respect to grooving and agglomeration. In particular, it has been shown that axiotaxy provide an efficient way to promote agglomeration because the interface can be bent without too much energy cost. The model with a circular segment geometry is in agreement with axiotaxy which is expected to lead essentially to a two-dimensional interface bending along the direction of the matching plane with a constant curvature. In the perpendicular direction, a non-special interface should limit bending of the interface and thus limit agglomeration. Our work shows that the diffusion of the slow diffusing species has to be taken into account in models for dewetting of compounds. The understanding of the dewetting of compound films should be of great importance for the nanostructuration of thin films [7] [43] [44] [45] [46] and/or for the growth of nanostructures [47] [48]. On the other hand, diffusion along interfaces is also crucial for applications [49]

[50] [51] but difficult to measure [52] [53] [54]. The method developed here (dewetting coupled with isotope distribution measured by APT) may also provide a way to measure diffusion at the interface in compounds.

5. Conclusions

The 3D redistribution of Si isotopes has been determined by APT for an agglomerated film of NiSi obtained by the reaction between a 15 nm Ni film and a Si isotope multilayer. The multilayer structure is maintained in some regions of NiSi showing a limited diffusion in NiSi. In other regions of either NiSi or Si, the isotopes are fully mixed. Comparison with a model assuming that mixing of Si isotope occurs by self-diffusion at the NiSi/Si interface allows reproducing the main features of the isotope redistribution. Our work demonstrates that diffusion of the less mobile species is of crucial importance for agglomeration of compounds. The finding of this fundamental mechanism brings a new understanding of the dewetting of compound films that is of great importance for the nanostructuration of thin films and/or for the growth of nanostructures. Indeed quantitative prediction of dewetted shapes requires improved models and simulations of dewetting through the knowledge of the mechanism. The results reported here and the associated model provide a new way for simulations of dewetting and thus for producing complex structures.

Acknowledgements

The French ministry for education and research is acknowledged for providing the scholarship for the PhD of T. Luo. The authors would like to thank Marion Descoins and Maxime

Bertoglio for technical assistance, Andrea Campos for the BSE and EDS characterization, Eugene E. Haller (Lawrence Berkeley National Laboratory, Berkeley, USA) for providing the stable, highly enriched Si isotopes and John Lundsgaard Hansen (University of Aarhus, Denmark) for the MBE growth of the Si isotope structure. P. Jacquet and V. Derkach are acknowledged for fruitful discussions.

References

[1] C. Lavoie, F.M. d'Heurle, C. Detavernier, C. Cabral, Towards implementation of a nickel silicide process for CMOS technologies, Microelectron. Eng. 70 (2003) 144–157. doi:10.1016/S0167-9317(03)00380-0.

[2] D. Deduytsche, C. Detavernier, R.L. Van Meirhaeghe, C. Lavoie, High-temperature degradation of NiSi films: Agglomeration versus NiSi[sub 2] nucleation, J. Appl. Phys. 98 (2005) 033526. doi:10.1063/1.2005380.

[3] B. Legrand, V. Agache, J.P. Nys, V. Senez, D. Stievenard, Formation of silicon islands on a silicon on insulator substrate upon thermal annealing, Appl. Phys. Lett. 76 (2000) 3271–3273. doi:10.1063/1.126603.

[4] C. Jahan, O. Faynot, L. Tosti, J.M. Hartmann, Agglomeration control during the selective epitaxial growth of Si raised sources and drains on ultra-thin silicon-on-insulator substrates, J. Cryst. Growth. 280 (2005) 530–538. doi:10.1016/j.jcrysgro.2005.03.088.

[5] J. Becker, G. Grün, R. Seemann, H. Mantz, K. Jacobs, K.R. Mecke, R. Blossey, Complex dewetting scenarios captured by thin-film models, Nat. Mater. 2 (2003) 59–63. doi:10.1038/nmat788.

[6] J. Huang, F. Kim, A.R. Tao, S. Connor, P. Yang, Spontaneous formation of nanoparticle stripe patterns through dewetting, Nat. Mater. 4 (2005) 896–900. doi:10.1038/nmat1517.

[7] L.-X. Lu, Y.-M. Wang, B.M. Srinivasan, M. Asbahi, J.K.W. Yang, Y.-W. Zhang, Nanostructure Formation by controlled dewetting on patterned substrates: A combined theoretical, modeling and experimental study, Sci. Rep. 6 (2016) 32398. doi:10.1038/srep32398.

[8] M. Naffouti, R. Backofen, M. Salvalaglio, T. Bottein, M. Lodari, A. Voigt, T. David, A. Benkouider, I. Fraj, L. Favre, A. Ronda, I. Berbezier, D. Grosso, M. Abbarchi, M. Bollani, Complex dewetting scenarios of ultrathin silicon films for large-scale nanoarchitectures, Sci. Adv. 3 (2017) eaao1472. doi:10.1126/sciadv.aao1472.

[9] C.V. Thompson, Solid-State Dewetting of Thin Films, in: D.R. Clarke (Ed.), Annu. Rev. Mater. Res. Vol 42, 2012: pp. 399–434.

[10] F. Leroy, L. Borowik, F. Cheynis, Y. Almadori, S. Curiotto, M. Trautmann, J.C. Barbe, P. Mueller, How to control solid state dewetting: A short review, Surf. Sci. Rep. 71 (2016) 391–409. doi:10.1016/j.surfrep.2016.03.002.

[11] W.W. Mullins, Theory of Thermal Grooving, J. Appl. Phys. 28 (1957) 333–339. doi:10.1063/1.1722742.

[12] D. Srolovitz, S. Safran, Capillary Instabilities in Thin-Films .1. Energetics, J. Appl. Phys. 60 (1986) 247–254. doi:10.1063/1.337689.

[13] D. Srolovitz, S. Safran, Capillary Instabilities in Thin-Films .2. Kinetics, J. Appl. Phys. 60 (1986) 255–260. doi:10.1063/1.337691.

[14] K.T. Miller, F.F. Lange, D.B. Marshall, The instability of polycrystalline thin films: Experiment and theory, J. Mater. Res. 5 (1990) 151–160. doi:10.1557/JMR.1990.0151.

[15] T.P. Nolan, R. Sinclair, R. Beyers, Modeling of agglomeration in polycrystalline thin films: Application to TiSi2 on a silicon substrate, J. Appl. Phys. 71 (1992) 720. doi:10.1063/1.351333.

[16] O. Kovalenko, J.R. Greer, E. Rabkin, Solid-state dewetting of thin iron films on sapphire substrates controlled by grain boundary diffusion, Acta Mater. 61 (2013) 3148–3156. doi:10.1016/j.actamat.2013.01.062.

[17] V. Derkach, A. Novick-Cohen, A. Vilenkin, E. Rabkin, Grain boundary migration and grooving in thin 3-D systems, Acta Mater. 65 (2014) 194–206. doi:10.1016/j.actamat.2013.10.061.

[18] P. Jacquet, R. Podor, J. Ravaux, J. Teisseire, I. Gozhyk, J. Jupille, R. Lazzari, Grain growth: The key to understand solid-state dewetting of silver thin films, Scr. Mater. 115 (2016) 128–132. doi:10.1016/j.scriptamat.2016.01.005.

[19] P. Jacquet, R. Podor, J. Ravaux, J. Lautru, J. Teisseire, I. Gozhyk, J. Jupille, R. Lazzari, On the solid-state dewetting of polycrystalline thin films: Capillary versus grain growth approach, Acta Mater. 143 (2018) 281–290. doi:10.1016/j.actamat.2017.08.070.

[20] A. Kosinova, L. Klinger, O. Kovalenko, E. Rabkin, The role of grain boundary sliding in solid-state dewetting of thin polycrystalline films, Scr. Mater. 82 (2014) 33–36. doi:10.1016/j.scriptamat.2014.03.015.

[21] A. Kosinova, O. Kovalenko, L. Klinger, E. Rabkin, Mechanisms of solid-state dewetting of thin Au films in different annealing atmospheres, Acta Mater. 83 (2015) 91–101. doi:10.1016/j.actamat.2014.09.049.

[22] H. Jeon, C.A. Sukow, J.W. Honeycutt, G.A. Rozgonyi, R.J. Nemanich, Morphology and phase stability of TiSi2 on Si, J. Appl. Phys. 71 (1992) 4269–4276. doi:10.1063/1.350808.

[23] S.L. Hsia, T.Y. Tan, P. Smith, G.E. McGuire, Resistance and structural stabilities of epitaxial CoSi2 films on (001) Si substrates, J. Appl. Phys. 72 (1992) 1864–1873. doi:10.1063/1.351659.

[24] E.G. Colgan, J.P. Gambino, Q.Z. Hong, Formation and stability of silicides on polycrystalline silicon, Mater. Sci. Eng. R-Rep. 16 (1996) 43–96. doi:10.1016/0927-796X(95)00186-7.

[25] F.A. Geenen, K. van Stiphout, A. Nanakoudis, S. Bals, A. Vantomme, J. Jordan-Sweet, C. Lavoie, C. Detavernier, Controlling the formation and stability of ultra-thin nickel silicides - An alloying strategy for preventing agglomeration, J. Appl. Phys. 123 (2018) 075303. doi:10.1063/1.5009641.

[26] M. Bouville, S.Y. Hu, L.Q. Chen, D.Z. Chi, D.J. Srolovitz, Phase-field model for grain boundary grooving in multi-component thin films, Model. Simul. Mater. Sci. Eng. 14 (2006) 433–443. doi:10.1088/0965-0393/14/3/007.

[27] C. Detavernier, A.S. Ozcan, J. Jordan-Sweet, E.A. Stach, J. Tersoff, F.M. Ross, C. Lavoie, An off-normal fibre-like texture in thin films on single-crystal substrates, Nature. 426 (2003) 641–645. doi:10.1038/nature02198.

[28] D. Mangelinck, J.Y. Dai, J.S. Pan, S.K. Lahiri, Enhancement of thermal stability of NiSi films on (100)Si and (111)Si by Pt addition, Appl. Phys. Lett. 75 (1999) 1736–1738. doi:10.1063/1.124803.

[29] D. Deduytsche, C. Detavernier, R.L. Van Meirhaeghe, J.L. Jordan-Sweet, C. Lavoie, Formation and morphological stability of NiSi in the presence of W, Ti, and Ta alloying elements, J. Appl. Phys. 101 (2007) 044508. doi:10.1063/1.2433133.

[30] C. Lavoie, C. Detavernier, C. Cabral, F.M. d'Heurle, A.J. Kellock, J. Jordan-Sweet, J.M.E. Harper, Effects of additive elements on the phase formation and morphological

stability of nickel monosilicide films, Microelectron. Eng. 83 (2006) 2042–2054. doi:10.1016/j.mee.2006.09.006.

[31] C. Detavernier, C. Lavoie, Influence of Pt addition on the texture of NiSi on Si(001), Appl. Phys. Lett. 84 (2004) 3549. doi:10.1063/1.1719276.

[32] M. Bouville, D. Chi, D.J. Srolovitz, Grain-boundary grooving and agglomeration of alloy thin films with a slow-diffusing species, Phys. Rev. Lett. 98 (2007) 085503. doi:10.1103/PhysRevLett.98.085503.

[33] D. Mangelinck, F. Panciera, K. Hoummada, M. El Kousseifi, C. Perrin, M. Descoins, A. Portavoce, Atom probe tomography for advanced metallization, Microelectron. Eng. 120 (2014) 19–33. doi:10.1016/j.mee.2013.12.018.

[34] M.-A. Nicolet, S.S. Lau, Chapter 6 - Formation and Characterization of Transition-Metal Silicides, in: N.G. Einspruch, G.B. Larrabee (Eds.), VLSI Electron. Microstruct. Sci., Elsevier, 1983: pp. 329–464. doi:10.1016/B978-0-12-234106-9.50011-8.

[35] O. Nakatsuka, K. Okubo, A. Sakai, M. Ogawa, Y. Yasuda, S. Zaima, Improvement in NiSi/Si contact properties with C-implantation, Microelectron. Eng. 82 (2005) 479–484. doi:10.1016/j.mee.2005.07.046.

[36] A. Lauwers, J.A. Kittl, M.J.H. Van Dal, O. Chamirian, M.A. Pawlak, M. de Potter, R. Lindsay, T. Raymakers, X. Pages, B. Mebarki, T. Mandrekar, K. Maex, Ni based silicides for 45 nm CMOS and beyond, Mater. Sci. Eng. B. 114–115 (2004) 29–41. doi:10.1016/j.mseb.2004.07.028.

[37] H. Benallali, K. Hoummada, M. Descoins, P. Rueda-Fonseca, L. Gerard, E. Bellet-Amalric, S. Tatarenko, K. Kheng, D. Mangelinck, Nature of the ZnSe/GaAs interface investigated by atom probe tomography, Scr. Mater. 69 (2013) 505–508. doi:10.1016/j.scriptamat.2013.05.041.

[38] B. Gault, M.P. Moody, J.M. Cairney, S.P. Ringer, Atom Probe Microscopy, Springer Science & Business Media, 2012.

[39] H. Bracht, E.E. Haller, R. Clark-Phelps, Silicon Self-Diffusion in Isotope Heterostructures, Phys. Rev. Lett. 81 (1998) 393–396. doi:10.1103/PhysRevLett.81.393.

[40] O. Pierre-Louis, A. Chame, Y. Saito, Dewetting of Ultrathin Solid Films, Phys. Rev. Lett. 103 (2009) 195501. doi:10.1103/PhysRevLett.103.195501.

[41] R.V. Zucker, G.H. Kim, W. Craig Carter, C.V. Thompson, A model for solid-state dewetting of a fully-faceted thin film, Comptes Rendus Phys. 14 (2013) 564–577. doi:10.1016/j.crhy.2013.06.005.

[42] D. Amram, L. Klinger, N. Gazit, H. Gluska, E. Rabkin, Grain boundary grooving in thin films revisited: The role of interface diffusion, Acta Mater. 69 (2014) 386–396. doi:10.1016/j.actamat.2014.02.008.

[43] J. Quan, J. Zhang, X. Qi, J. Li, N. Wang, Y. Zhu, A study on the correlation between the dewetting temperature of Ag film and SERS intensity, Sci. Rep. 7 (2017) 14771. doi:10.1038/s41598-017-15372-y.

[44] J. Ye, Fabrication of ordered arrays of micro- and nanoscale features with control over their shape and size via templated solid-state dewetting, Sci. Rep. 5 (2015) 9823. doi:10.1038/srep09823.

[45] M. Kang, S.-G. Park, K.-H. Jeong, Repeated Solid-state Dewetting of Thin Gold Films for Nanogap-rich Plasmonic Nanoislands, Sci. Rep. 5 (2015) 14790. doi:10.1038/srep14790.

[46] J. Ye, C.V. Thompson, Templated Solid-State Dewetting to Controllably Produce Complex Patterns, Adv. Mater. 23 (2011) 1567–1571. doi:10.1002/adma.201004095.

[47] F. Panciera, Y.-C. Chou, M.C. Reuter, D. Zakharov, E.A. Stach, S. Hofmann, F.M. Ross, Synthesis of nanostructures in nanowires using sequential catalyst reactions, Nat. Mater. 14 (2015) 820–825. doi:10.1038/nmat4352.

[48] S. Hofmann, R. Sharma, C.T. Wirth, F. Cervantes-Sodi, C. Ducati, T. Kasama, R.E. Dunin-Borkowski, J. Drucker, P. Bennett, J. Robertson, Ledge-flow-controlled catalyst interface dynamics during Si nanowire growth, Nat. Mater. 7 (2008) 372–375. doi:10.1038/nmat2140.

[49] J. Garcia-Barriocanal, A. Rivera-Calzada, M. Varela, Z. Sefrioui, E. Iborra, C. Leon, S.J. Pennycook, J. Santamaria, Colossal ionic conductivity at interfaces of epitaxial ZrO2:Y2O3/SrTiO3 heterostructures, Science. 321 (2008) 676–680. doi:10.1126/science.1156393.

[50] J.R. Lloyd, J.J. Clement, Electromigration in copper conductors, Thin Solid Films. 262 (1995) 135–141. doi:10.1016/0040-6090(94)05806-7.

[51] M.W. Lane, E.G. Liniger, J.R. Lloyd, Relationship between interfacial adhesion and electromigration in Cu metallization, J. Appl. Phys. 93 (2003) 1417–1421. doi:10.1063/1.1532942.

[52] A. Paul, S. Divinski, Handbook of Solid State Diffusion, 2017.

[53] I. Kaur, Y. Mishin, W. Gust, Fundamentals of Grain and Interphase Boundary Diffusion, Wiley, 1995.

[54] S.V. Divinski, F. Hisker, A. Bartels, C. Herzig, Interphase boundary diffusion of 44Ti in two-phase TiAl with lamellar α2/γ structure, Scr. Mater. 45 (2001) 161–167. doi:10.1016/S1359-6462(01)01006-5.

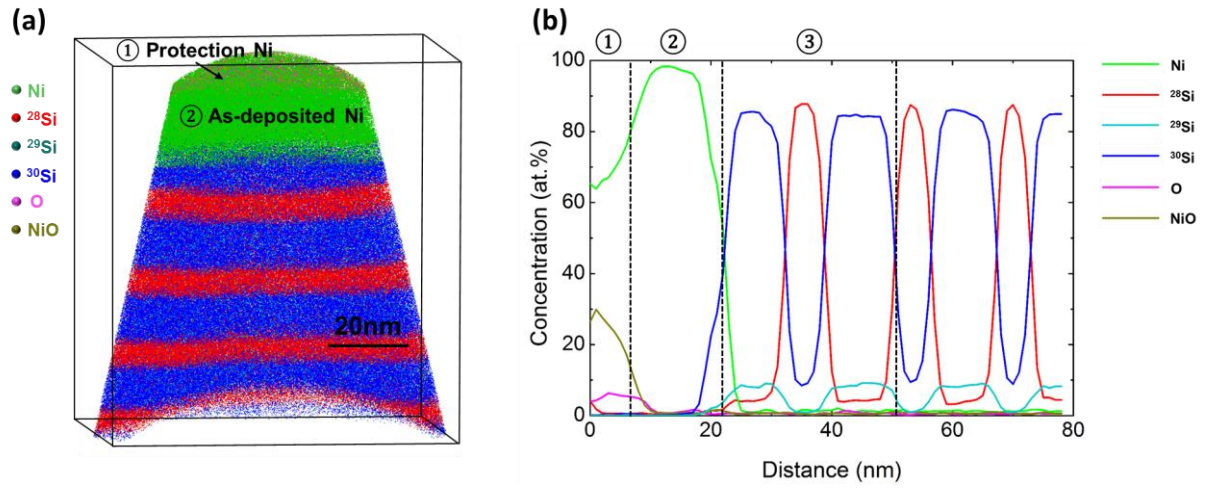

Figure 1: APT analysis of the as-deposited 15nm Ni film deposited on the Si isotope multilayer: (a) APT volume showing the Ni protection layer, the as-deposited 15nm-Ni film and the Si isotope multilayer, (b) 1D concentration depth profile in a 10nm-diameter cylinder perpendicular to the interface and locating in the center of the volume. Region-① represents the protection Ni layer which contains a high content of oxygen and oxide. Region-② is the as-deposited 15nm Ni layer and Region-③ corresponds to the expected thickness of the Si multilayer consumed by the 15nm Ni for the NiSi formation.

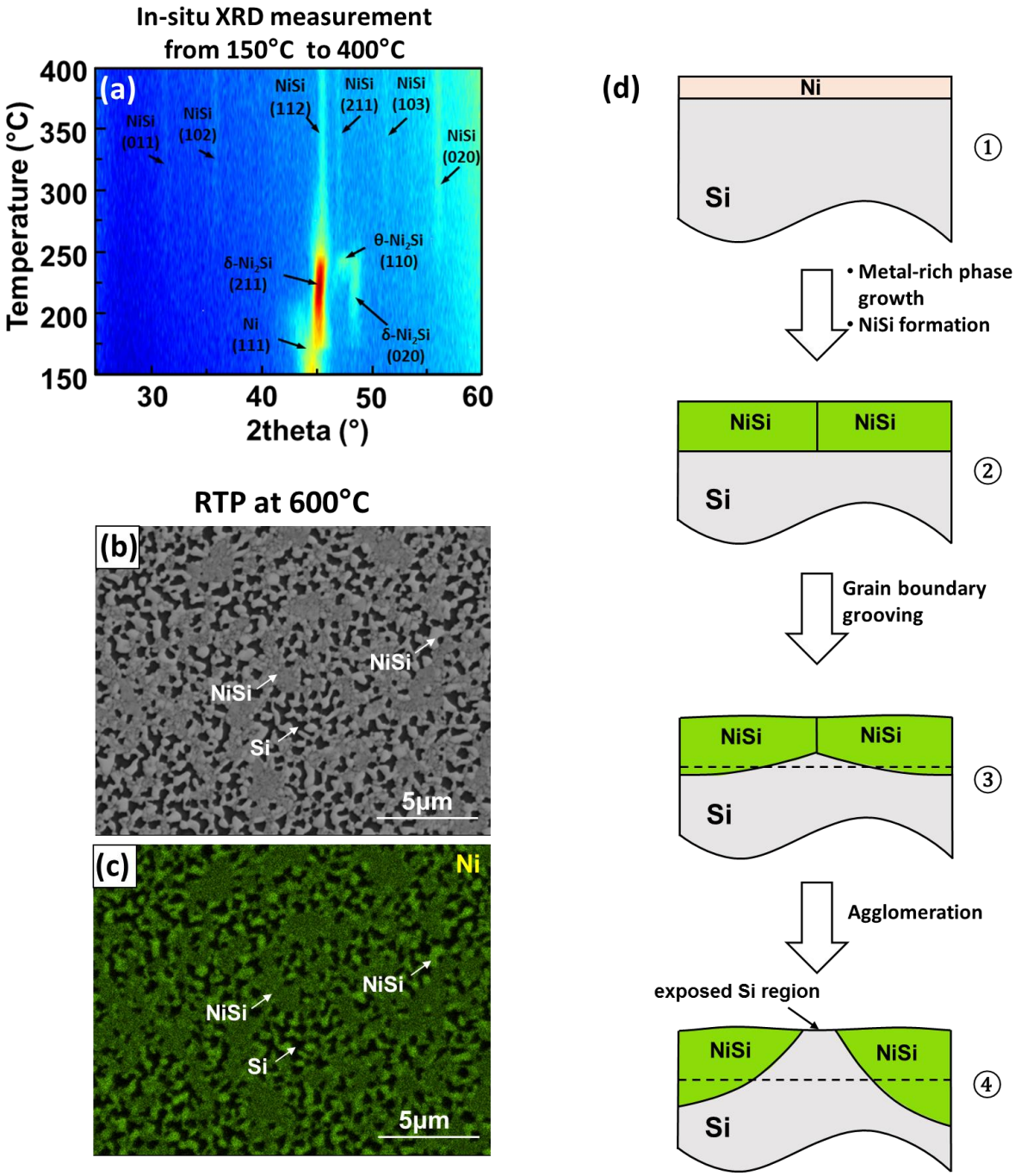

Figure 2: (a) In-situ XRD measurement of a15nm Ni/Si sample from 150 °C to 400 °C, showing that NiSi is the unique phase at 400°C. (b) Top-view BSE image of a 600°C-annealed 15 nm Ni/Si sample and (c) the corresponding EDS map of Ni, where agglomerated NiSi regions and exposed Si regions are observed. (d) Schematic showing the formation, the grain boundary grooving and the agglomeration of NiSi.

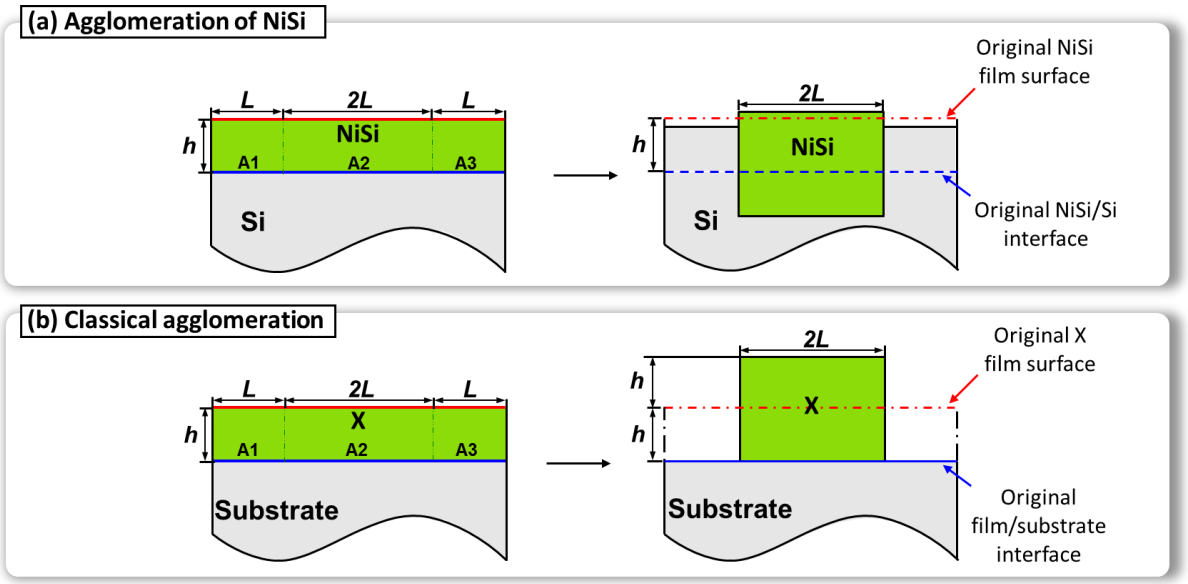

Figure 3. Schematic comparing (a) the NiSi agglomeration and (b) the classical agglomeration of a mono-component film (X). For each film, one grain with an area of $h \times 4l$ is considered, where h is the original thickness of the non-agglomerated film and $4l$ corresponds to the grain size before agglomeration. Region *A1* and *A3* refer to one quarter of the area ($h \times l$) while region *A2* equals to half of the area ($h \times 2l$).

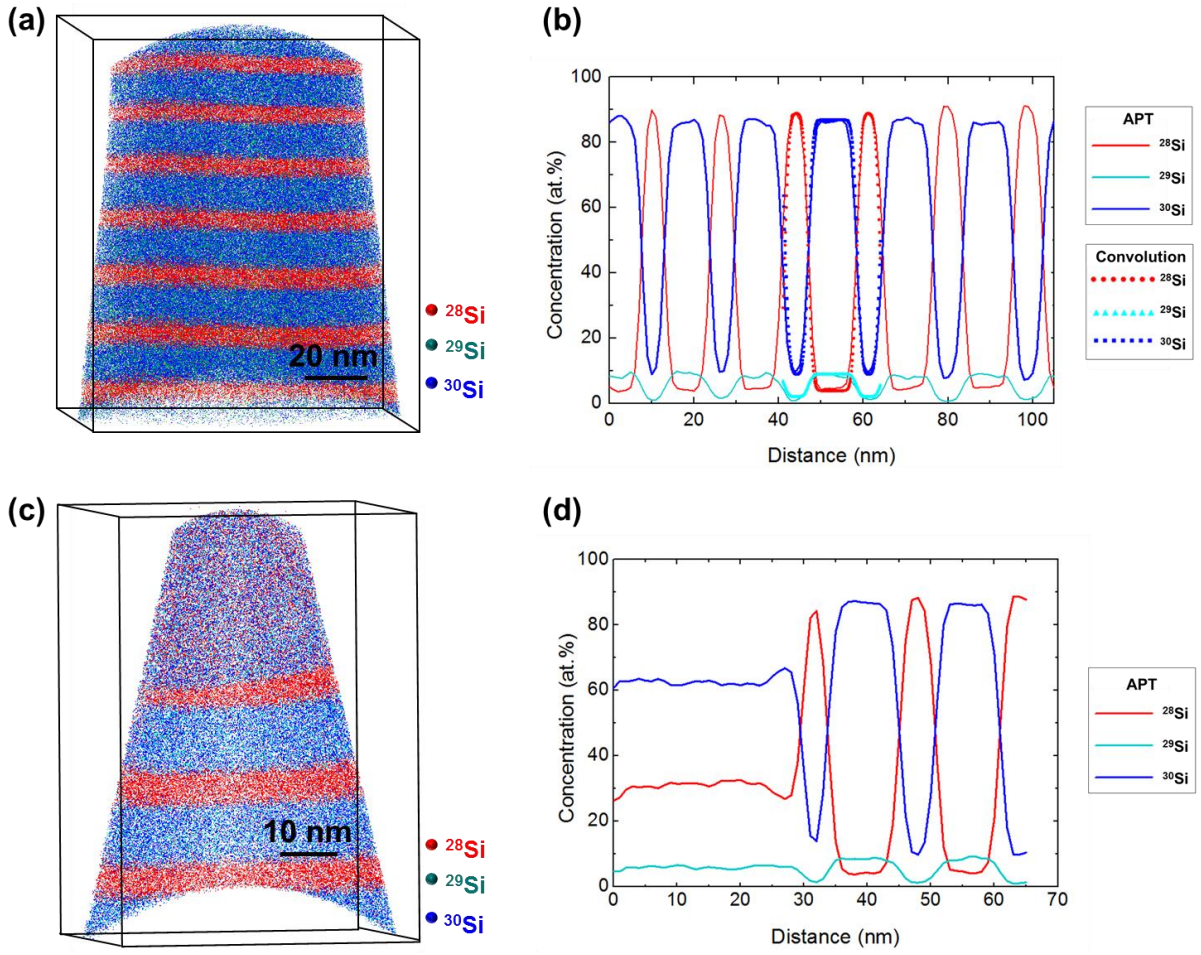

Figure 4: APT analysis of Si regions of the 15nm Ni film on the Si isotope multilayer after annealing at 600°C: (a) APT volume showing the multilayer structure of isotope Si(001), (b) 1D concentration depth profile in a 10nm-diameter cylinder perpendicular to the interface and locating in the center of the volume. In order to determine the composition and thickness of the individual bilayer (^{30}Si rich layer and ^{28}Si rich layer), a theoretical profile with constant concentration and sharp interface was convoluted by a Gaussian with a 2 nm FHWM (dotted line in the center of (b)). (c) APT volume showing a mixed Si layer on top of the original isotope multilayer of Si. (d) 1D concentration depth profile in a 10nm-diameter cylinder perpendicular to the interface.

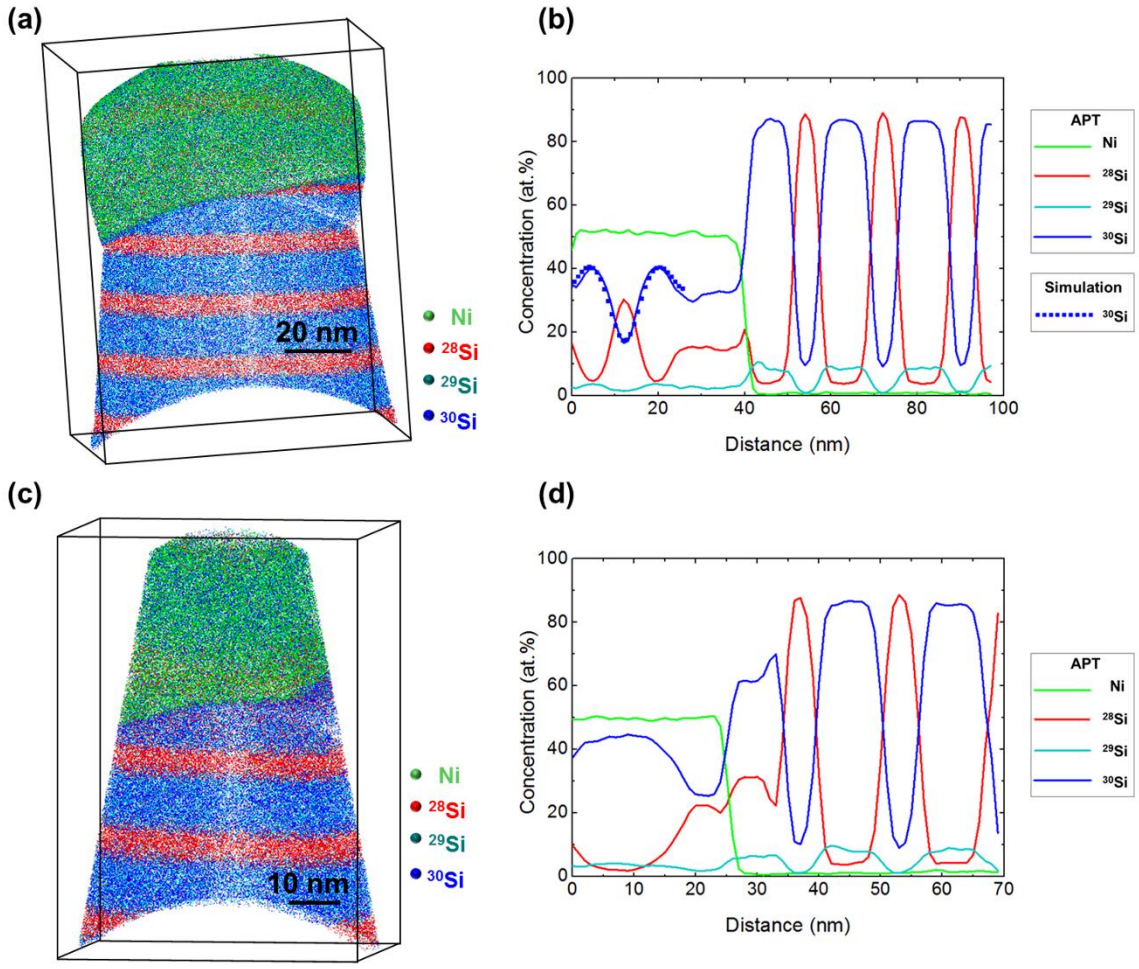

Figure 5: APT analysis of regions covered by NiSi of the 15nm Ni film on the Si isotope multilayer after annealing at 600°C: (a) one APT volume with a layered NiSi/ mixed NiSi / layered Si structure; (b) 1D concentration depth profile in a 10nm-diameter cylinder perpendicular to the interface. The ^{30}Si profile taking into account the self-diffusion in NiSi simulated by finite difference is superimposed as doted points. (c) APT volume with three regions: a NiSi layer with layered Si isotopes, a mixed Si isotopes region and Si isotope multilayer. (d) 1D concentration depth profile in a 10nm-diameter cylinder perpendicular to the interface.

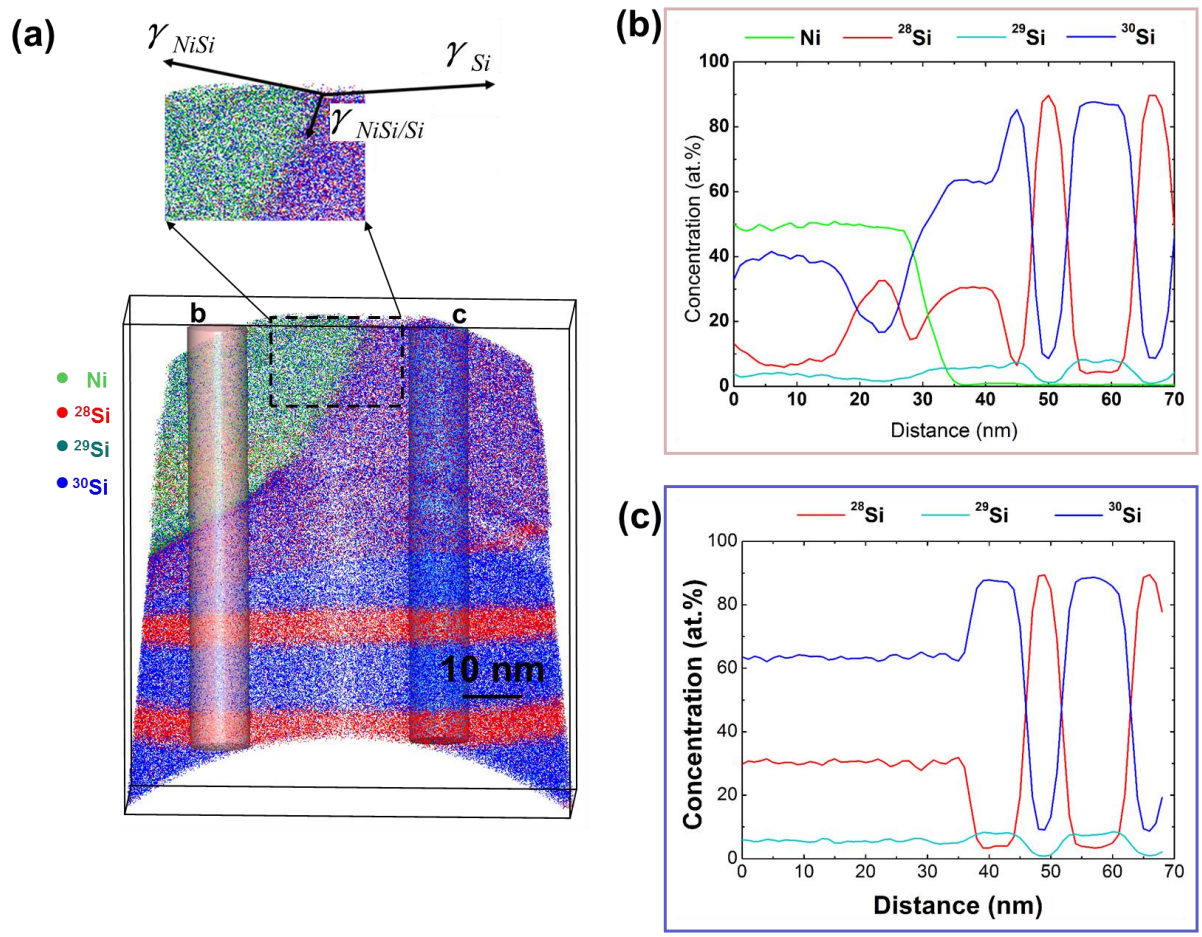

Figure 6: APT analysis of the region with NiSi and Si at the surface of the 15nm Ni film on the Si isotope multilayer after annealing at 600°C: (a) APT volume showing the boundary between the agglomerated NiSi and the exposed Si substrate. Si isotopes are in a layered structure in NiSi while a mixed layer of Si isotopes is found on the top of the original isotope multilayer of Si. The region, indexed by the dashed box, is extracted to show schematically the relationship of NiSi surface energy, Si surface energy and NiSi/Si interface energy. (b) and (c) corresponds to the 1D concentration depth profiles in a 10nm-diameter cylinder crossing the region of NiSi (pink cylinder on the left) or Si (blue cylinder on the right), respectively.

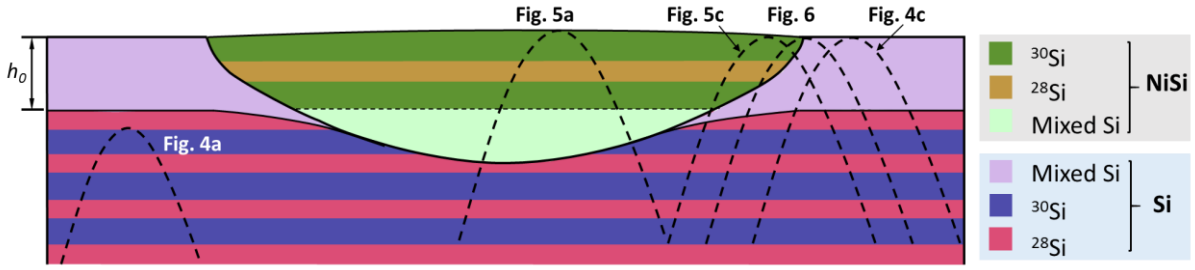

Figure 7: Schematic diagram showing the agglomeration of the 15 nm Ni film deposited on the Si isotope multilayer after annealing at 600°C. *h* is the NiSi films thickness expected for the 15nm Ni film (~33nm). Depending on the state of isotope Si atoms inside NiSi and Si substrate (mixed or layered), five different structures were observed in APT and the corresponding positions are shown.

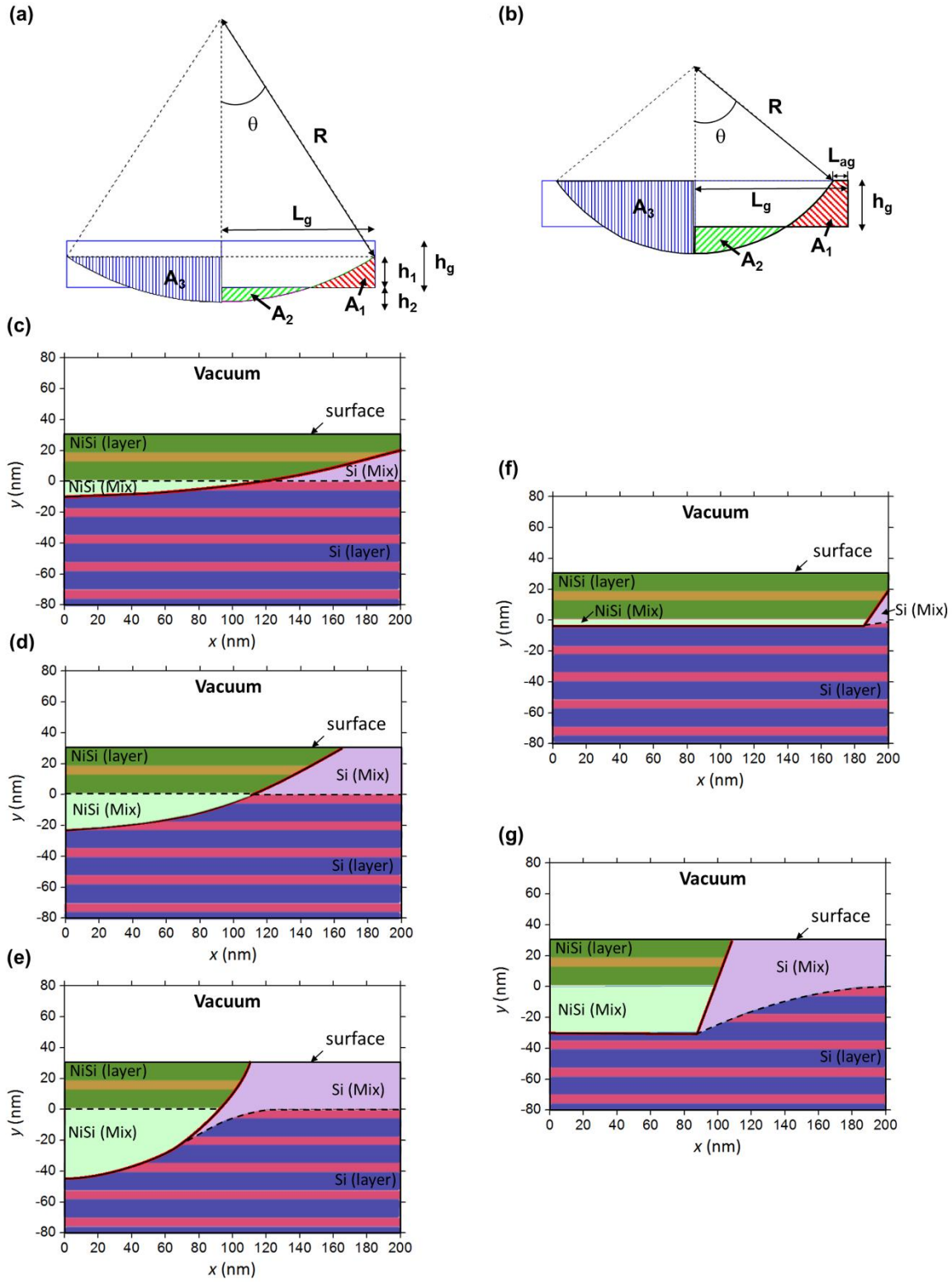

Figure 8: Models and simulation for the grooving and agglomeration: Schematic of the model based on a circular segment geometry used to simulate the mixing of the Si isotope during grooving (a) and agglomeration (b). *R* and *θ* correspond to the radius of the NiSi/Si interface

curvature and the angle defining the circular segment geometry. L_g and h_g are the half size of the NiSi grain and the original thickness of the non-agglomerated NiSi film. h_1 and h_2 are the depth of the grain boundary grooving and the depth of the newly formed NiSi. L_{ag} is the agglomerated length. Simulation based on a circular segment geometry, showing the mixing of the Si isotope during grooving and agglomeration: (c) grooving, (d) beginning of agglomeration, and (e) later stage of agglomeration. Simulation of a facetted NiSi grain, showing the mixing of the Si isotope during (f) grooving and (g) agglomeration.